A Grid Interface Current Control Strategy for DC Microgrids

Muhannad Alshareef, Zhengyu Lin, *Senior Member, IEEE*, Fulong Li, *Member, IEEE,* and Fei Wang, *Senior Member, IEEE*

***Abstract*—In this paper, a grid interface current control strategy is presented for a DC microgrid, which aims to reduce the disturbance from PV generation and the load variation to the main grid without a grid interface converter. The grid interface current is directly controlled by a battery DC-DC converter within the DC microgrid. Based on a comprehensive analysis of the battery DC-DC converter and interface current control, the control system has been mathematically modelled. This enabled two transfer functions to be derived that reflect the dynamic response of the inductor current to the duty cycle variation (inner loop), and the dynamic response of the grid interface current to the inductor current variation (outer loop). Experimental study has been done to assess the effectiveness of the proposed control strategy. The experimental results indicate that the proposed control strategy has a good performance to control the grid interface current without an interface converter, regardless the variations of both PV and the load conditions.**

***Index Terms*— Battery, DC microgrid, DC-DC converter, photovoltaic (PV) system.**

I. INTRODUCTION

DISTRIBUTED generation (DG) plays an important role in modern power systems, which includes renewable energy resources, energy storage systems and innovative types of load, such as electric vehicles. However, without a proper coordinated operation, it will cause a variety of issues to power systems, such as degraded voltage profiles, congestion in the transmission line and a decrease in frequency reserves [1].

To accommodate more DGs in power grids and reduce carbon emission, structured microgrids have been recognized as the key energy infrastructure for future smart energy systems [2]. Microgrid components can be connected through direct current (DC) links or alternating current (AC) links. With the development of power electronics technologies, DC energy systems have gained an increasing research interest in the last few years. DC based energy systems have a natural interface to DC renewable generation, energy storage and DC electronics loads [3]. Compared with conventional AC systems, DC systems have advantages of simpler control, higher reliability and efficiency [4]-[6].

In [7], the effects of a renewable source within the microgrid on LV distribution network operation were investigated. Simulations of daily PV and load profiles were made to analyze fluctuations in utility voltage and line losses. This research given valuable insight into the operation of PV microgrids in weak LV networks. The findings indicated that the utility voltage was impacted by PV and load fluctuations, while line losses in the LV network were also observed. The authors determined that it was essential to utilize an advanced controller for eliminating these fluctuations [7].

In the study conducted in [8], an interleaved interface converter was designed for the purposes of controlling the power flow between a DC microgrid and the DC bus of a main DC grid. The controller was designed to be more effective to prevent PV and load disturbances instead of just tracking the reference provided. In order to ensure that the DC bus voltage remains at a constant level, it is important to ensure that the PV and load variations that are generated within a DC microgrid are managed efficiently. Such variations can lead to a series of voltage variations, which could be transferred to sensitive loads. However, this study requires a DC/DC interleaved converter to act as the interface connecting between the DC microgrid and the main DC grid, which could increase the cost of the system.

The researchers in [9] presented a novel power balancing approach that could be used for low voltage DC microgrids. The study was aimed at extracting the MPP from the PV, while simultaneously mitigating the effects of fluctuations of PV output power on the main AC grid. Additionally, a supervision layer was developed for the purpose of optimizing the usage of the battery energy storage system (BESS), thus compensating for any increase/decrease in voltage caused by the droop controller.

Also, microgrids can significantly benefit via the participation in pricing between supply and demand. As suggested in [10], an aggregator is an organization that collects the power generated by multiple microgrids and then sells that

Manuscript received August 18, 2020; revised January 22, 2021; accepted March 09, 2021. date of publication September 25, 2021; date of current version September 18, 2021.

This work has received funding from the U.K. EPSRC UKRI Innovation Fellowship scheme (EP/S001662/2), and the European Union's Horizon 2020 research and innovation programme under grant agreement No.734796.

M. Alshareef is with Department of Electronics and Communication Engineering in Al-Qunfudhah, Umm al-Qura University, Makkah, Saudi Arabia (email: mjshareef@uqu.edu.sa)

Z. Lin and F. Li are with the School of Mechanical, Electrical and Manufacturing Engineering, Loughborough University, Loughborough, LE11 3TU, United Kingdom (e-mail: Z.Lin@ieee.org and F.Li@lboro.ac.uk)

F. Wang is with the School of Mechatronic Engineering and Automation, Shanghai University, Baoshan District, Shanghai 200444, China (email: f.wang@shu.edu.cn)

(Corresponding Author: Zhengyu Lin)

Digital Object Identifier 10.30941/CESTEMS.2021.00028

2096-3564 © 2021 CES

power to the utility with the aim of achieving better prices. Thus, it is desirable for microgrids to deliver power to the utility based on the aggregator's request, regardless of the intermittent nature of the renewable generation and load demand variations.

In this study, a DC microgrid interface current control strategy is proposed for the DC distribution network to ensure that PV and load disturbances are not transferred to the main DC grid. The proposed interface current control strategy is based on the power converter control for the battery energy storage within the DC microgrid, and no additional interface converter is required between the DC microgrid and the main DC grid. Consequently, the costs of the system can be reduced while still maintaining a similar control performance to that demonstrated in [8].

The rest of this paper is organized as follows: Section II presents the DC microgrid system configuration used in this study. The small signal modelling of the system is described in Section III. Section IV explains the proposed control strategy along with the compensators design. Section V reports the experimental findings and the paper ends with conclusions in Section VI.

II. CONFIGURATION OF THE DC MICROGRID SYSTEM

The block diagram of the DC microgrid system employed in this study is shown in Fig. 1. The DC microgrid is connected to the DC main grid without grid interface converter. All the converters within the DC microgrid work at current mode, so the DC microgrid as a whole is connected to the DC main grid at current mode. By control the interface current I_m, the power flow can be controlled between the DC main grid and the DC microgrid.

Within the DC microgrid, the PV array is connected to the DC bus via a Boost converter. MPPT algorithm is used for tracking the maximum power for the PV array, therefore, the output power from the PV varies with the weather conditions. The batteries are linked to the DC bus using a bi-directional DC-DC converter. Load is connected to the DC bus directly, and the power consumption is changed based on user requirement.

With the development of DC microgrid technologies, it is expected that multiple DC microgrids will be connected to form a DC main grid. Individual DC microgrid can be connected to the DC main grids via different ways, for example, using a bi-directional DC/DC converter to control the power flow between the DC microgrid and main DC grid as proposed in [8]. In this study, as shown in Fig. 1, a power inductor is used as the interface between DC microgrid and DC main grid. A grid interface current control strategy is proposed so that the grid interface current I_m can be controlled without an interface converter. The variations of PV current I_{PV} and load current I_{Load} are considered as the disturbances for the grid interface current control.

III. SMALL SIGNAL MODELLING AND ANALYSIS

In order to develop the grid interface current control scheme, it is necessary to investigate the dynamic behavior of the bi-directional DC-DC converter used for batteries. This requires the analysis and derivation of a small signal model of a bi-directional converter, as well as the grid interface current control between the DC microgrid and the main DC grid. This will allow two transfer functions to be derived, which are representative of the dynamic response of the inductor current of the battery convertor to the duty cycle variation, as well as the dynamic response of the grid interface current to the inductor current variation. Subsequently, two transfer functions will be employed to design the proposed control scheme's double loop PI compensators. As suggested in [11], the bi-directional convertor's charging and discharging modes share the same transfer function provided by the converter. Hence, a unified controller can be tolerated in situations where the two switches are supplemented by a single controller. The Boost operation mode is selected in this study for the controller design. The bi-directional DC-DC converter is shown in Fig. 2.

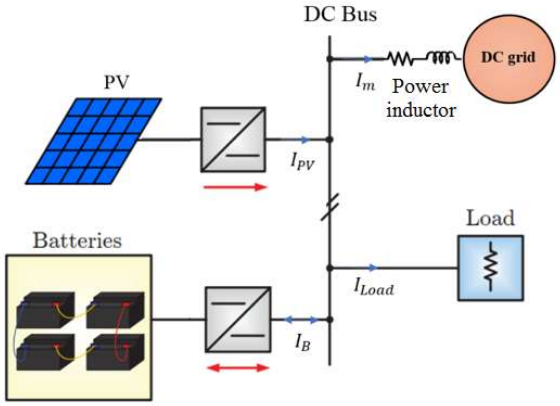

Fig. 1. The DC microgrid configuration for this study.

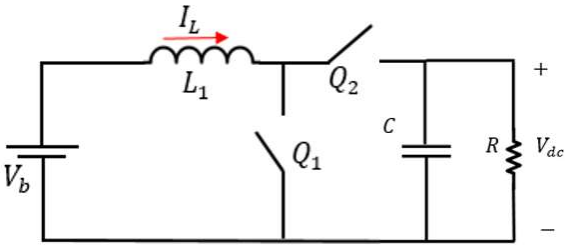

Fig. 2. The bi-directional DC-DC converter circuit diagram.

The general average equation for the inductor voltage of the power converter can be derived as:

$$\frac{d\hat{i}_L}{dt} = \frac{\hat{v}_b + V_{dc}\hat{d} - (1-D)\hat{v}_{dc}}{L_1} \tag{1}$$

where V_{dc}, L_1 and D denote the steady state variables of DC bus voltage, power converter inductor and duty cycle, respectively, while, $\hat{v}_{dc}$, $\hat{d}$ and $\hat{v}_b$ represent the small signal perturbation variables of DC bus voltage, duty cycle and battery voltage, respectively.

The general averaging equation of the capacitor current of the converter can be obtained as follows:

$$\frac{d\tilde{v}_{dc}}{dt}=\frac{(1-D)\hat{i}_L+I_L\hat{d}}{C}-\frac{\tilde{v}_{dc}}{RC} \tag{2}$$

where I_L, C, R, and D represent the steady state variables of inductor current, capacitance and the load resistance of power converter, and duty cycle whereas, $\tilde{v}_{dc}$, $\hat{i}_L$ and $\hat{d}$ denote the small signal perturbation variables of DC bus voltage, inductor current and duty cycle, respectively.

To simplify the analysis, the battery voltage V_b can be assumed as a constant, so that $\hat{v}_b$ is zero and can be ignored in the following analysis.

The Laplace transfer function of Equations (1) and (2) can be represented as follows:

$$s\hat{i}_L(s)=-\frac{1-D}{L_1}\tilde{v}_{dc}(s)+\frac{V_{dc}}{L_1}\hat{d}(s) \tag{3}$$

$$s\tilde{v}_{dc}(s)=\frac{1-D}{C}\hat{i}_L(s)-\frac{1}{RC}\tilde{v}_{dc}(s)-\frac{I_L}{C}\hat{d}(s) \tag{4}$$

By rearranging equations (3) and (4), the transfer functions of the inductor current to duty cycle variation $\hat{i}_L(s)/\hat{d}(s)$ and the DC bus voltage to duty cycle variation $\tilde{v}_{dc}(s)/\hat{d}(s)$ can be obtained:

$$\frac{\hat{i}_L(s)}{\hat{d}(s)}=\frac{V_{dc}Cs+2I_L(1-D)}{L_1Cs^2+\frac{L_1}{R}s+(1-D)^2} \tag{5}$$

$$\frac{\tilde{v}_{dc}(s)}{\hat{d}(s)}=\frac{-L_1I_Ls+(1-D)V_{dc}}{L_1Cs^2+\frac{L_1}{R}s+(1-D)^2} \tag{6}$$

Fig.3 shows a simplified diagram between the battery converter and the main DC grid. In this figure, V_{dc} depicts the DC bus voltage, I_L represents the inductor current, I_m denotes the grid interface current between the microgrid and the main DC grid, and V_m is the main DC grid voltage level. I_R is the sum of the generation and load currents within the microgrid. When I_R >0, it means the generation current is less than the load current, and when I_R <0, it means the generation current is higher than the load current. Fig.3 can be utilized in the derivation of the transfer function, which represents the dynamic response of the grid interface current I_m to inductor current variation I_L, I_R is the disturbance for the grid interface current control, and in this study, it is assumed I_R is small enough so that small signal model can be applied. For large variation of I_R , large signal model based control strategy need to be applied, which is not within the scope of this paper.

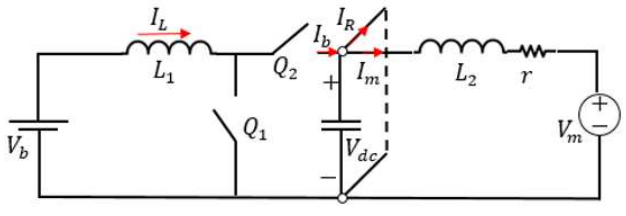

Fig.3. Simplified diagram of the battery converter with the grid interface current.

Based on Fig.3 the following Equation can be obtained:

$$i_m(s)=\frac{V_{dc}(s)-V_m(s)}{sL_2+r} \tag{7}$$

The assumption is made that $V_m(s)$ remains constant, meaning that its dynamic response can be ignored when the Equations are modelled.

By taking the derivative of equation (7):

$$\hat{i}_m(s)=\frac{\tilde{v}_{dc}(s)}{sL_2+r} \tag{8}$$

Rearrange equation (8)

$$\tilde{v}_{dc}(s)=\hat{i}_m(s)\times(sL_2+r) \tag{9}$$

By substituting Equation (9) into Equation (6):

$$\frac{\hat{i}_m(s)\times(sL_2+r)}{\hat{d}(s)}=\frac{-L_1I_Ls+(1-D)V_{dc}}{L_1Cs^2+\frac{L_1}{R}s+(1-D)^2}$$

So, the transfer function of the grid interface current to duty cycle variation $\hat{i}_m(s)/\hat{d}(s)$ can be obtained:

$$\frac{\hat{i}_m(s)}{\hat{d}(s)}=\frac{\tilde{v}_{dc}(s)}{\hat{d}(s)(sL_2+r)}=\frac{-L_1I_Ls+(1-D)V_{dc}}{\left[L_1Cs^2+\frac{L_1}{R}s+(1-D)^2\right]\times(sL_2+r)} \tag{10}$$

In this research, the transfer functions $\hat{i}_m(s)/\hat{i}_L(s)$ must be attained for designing a PI compensator of the grid interface current controller to do so the transfer function $\hat{i}_m(s)/\hat{i}_L(s)$ is obtained by the following relationship:

$$\frac{\hat{i}_m(s)}{\hat{i}_L(s)}=\frac{\hat{i}_m(s)}{\hat{d}(s)}\times\frac{\hat{d}(s)}{\hat{i}_L(s)} \tag{11}$$

By substituting Equation (5) and Equation (10) into Equation (11), the transfer function $\hat{i}_m(s)/\hat{i}_L(s)$ can be obtained as follow:

$$\frac{\hat{i}_m(s)}{\hat{i}_L(s)}=\frac{-L_1I_Ls+(1-D)V_{dc}}{\left[L_1Cs^2+\frac{L_1}{R}s+(1-D)^2\right]\times(sL_2+r)}\cdot\frac{L_1Cs^2+\frac{L_1}{R}s+(1-D)^2}{V_{dc}Cs+2I_L(1-D)}$$

$$\frac{\hat{i}_m(s)}{\hat{i}_L(s)}=\frac{-L_1I_Ls+(1-D)V_{dc}}{L_2CV_{dc}s^2+\left(2I_LL_2(1-D)+V_{dc}Cr\right)s+2I_L(1-D)r} \tag{12}$$

This equation describes the unique relationship between the grid interface current and the inductor current, and can be used later to design the outer current controller in the outer loop control section.

IV. THE PROPOSED CONTROL STRATEGY

In the proposed interface current control strategy, the charge/discharge current of the battery is controlled to prevent PV and load variations from being transferred to the main grid, and control the grid interface current between the DC microgrid and the main DC grid.

To control the grid interface current I_m a double loop interface current controller is developed, as shown in Fig.4. $I_{m_{ref}}$ is the reference current, which could be based on the request from an aggregator or a central controller. The reference current varies based on the request, but for a short period of time, it can be assumed as a constant.

The proposed controller structure is similar to the double loop voltage control for a single Boost converter. The inner control loop is responsible for regulating the battery converter inductor current. Instead of controlling the output voltage, the outer control loop in this controller is responsible for regulating the grid interface current.

The PV continually operates at maximum power point, and is therefore considered as a variable current source, whereas the DC load is regarded as a variable current sink. The variables G_{id}, G_{ii}, G_{pi_1}, G_{pi_2}, H_1, and H_2 represent the transfer function of the inner control loop, outer control loop, inner PI compensator, outer PI compensator, inner sensor and outer sensor, respectively.

A comparison is made between the grid interface current I_m and the reference current value $I_{m_{ref}}$; subsequently, the current error is delivered to the PI compensator G_{pi_2}, which generates the required current $I_{L_{ref}}$ for the inner control loop. A comparison is then made between the reference value $I_{L_{ref}}$ and the inductor current I_L and the current error is delivered to the PI compensator G_{pi_1}. After this, the PI compensator generates the required duty cycle D, which is transferred to the PWM generator in order to create switching pulses that correspond to the battery converter. The bandwidth of the inner current controller is fixed at approximately $f_{sw}/10$, where f_{sw} represents the switching device switching frequency, which is 25 kHz for this study.

The inner compensated control loop crossover frequency must be significantly lower than the main switching frequency. This is because the switching frequency can be rejected along with its related harmonics within the system control loop. Additionally, the outer control loop should have a slower response time in comparison to the inner control loop, as the former generates the reference for the latter and it must have greater speed to allow the inner control loop to track the generated reference by the outer control loop. Therefore, the bandwidth of the outer current control loop is maintained a level below that of the inner current control loop.

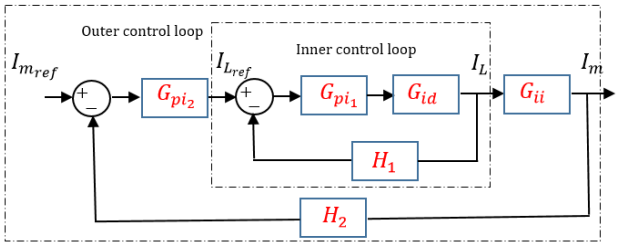

Fig.4. The proposed interface current control scheme.

A. Design of the inner current control loop

Fig.5 illustrates the block diagram of the inner current controller. The inductor reference current $I_{L_{ref}}$ is acquired from the outer control loop and subsequently moved to the inner current control loop.

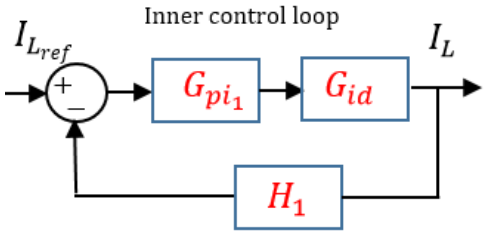

Fig.5. Inner current control block diagram.

The transfer function of G_{id} is given as follow:

$$G_{id} = \frac{\hat{i}_L(s)}{\hat{d}(s)} = \frac{V_{dc}Cs + 2I_L(1-D)}{L_1Cs^2 + \frac{L_1}{R}s + (1-D)^2} \tag{13}$$

The inner current control loop compensator G_{pi_1} transfer function is derived as:

$$G_{pi_1} = K_{p_1} + \frac{K_{i_1}}{s} \tag{14}$$

The open loop transfer function of the inner current control loop G_{ol_1} is formulated as:

$$G_{ol_1} = G_{id}G_{pi_1}H_1 \tag{15}$$

The transfer function of the closed loop gain G_{cl_1} is:

$$G_{cl_1} = \frac{G_{id}G_{pi_1}}{1 + G_{id}G_{pi_1}H_1} \tag{16}$$

Fig.6 shows the control block diagram, where the battery converter parameters used in the control design and experimental research are listed in Table I.

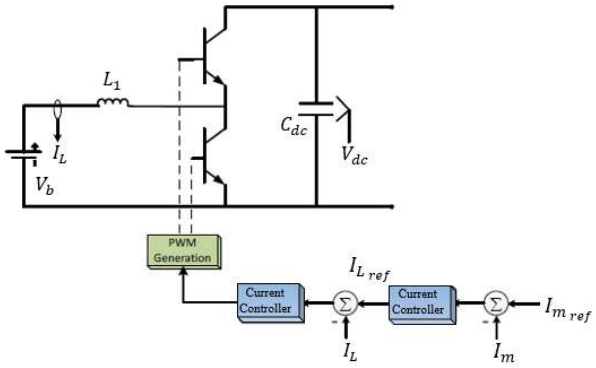

Fig.6. Battery converter control block diagram.

TABLE I
PARAMETERS AND OPERATING POINTS OF BATTERY CONVERTER

V_b (V)	I_L (A)	V_{dc} (V)	D	P (W)	R (Ω)	L_1 µH	L_2 µH	C_{dc} µF
24	8.3	48	0.5	200	100	240	240	470

The Bode plot for the compensated and uncompensated open loop transfer functions is represented in Fig.7. The design goal was to boost the low frequency loop gain in order to facilitate

the regulation of the output at a frequency lower than the loop crossover frequency. Hence, the objective was to boost the low frequency loop gain in order to reduce the steady state error in the output while maintaining a sufficient phase margin. The proportional integral (PI) compensator has the capability to manage this based on the parameter specifications, as the compensated loop gain of the inner control loop has a crossover frequency of 2.33 kHz and a phase margin of 63.2℃ . The calculated parameters of PI are formulated as: $K_{p_1} = 0.25$ and $K_{i_1} = 1800$.

B. Design of the outer current control loop

As shown in Fig.4, the transfer function of G_{ii} is given as follow:

$$G_{ii} = \frac{\hat{i}_m(s)}{\hat{i}_L(s)} = \frac{-L_1 I_L s + (1-D)V_{dc}}{L_2 C V_{dc} s^2 + (2I_L L_2 (1-D) + V_{dc} C r)s + 2I_L (1-D) r} \quad (17)$$

The transfer function of the outer current control loop compensator G_{pi_2} is given by:

$$G_{pi_2} = K_{p_2} + \frac{K_{i_2}}{s} \quad (18)$$

The open loop transfer function of outer current loop G_{ol_2} is given by:

$$G_{ol_2} = G_{ii} G_{pi_2} G_{cl_1} H_2 \quad (19)$$

The Bode plot for the compensated and uncompensated open loop transfer function is illustrated in Fig.8. The crossover frequency for the compensated loop gain of the outer control loop is 696 Hz and it has a phase margin of 64.5℃. The parameters formulated as: $K_{p_2} = 1.35$ and $K_{i_2} = 665$.

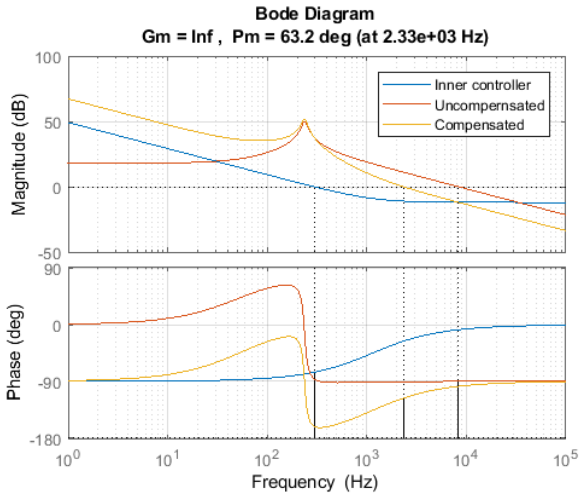

Fig. 7. Bode plot of the inner current control loop.

C. Controller Discretization

The two current compensators acquired above were based on S-domain. In a digital control system, the controller must be written in a discrete form. Hence, Tustin's method is used for z-mapping since it maintains stability and minimum margin for controller gain and phase characteristics. Using the Tustin's bilinear transformation method, the discrete controllers applied with sampling time T of 40μs can be expressed as follows:

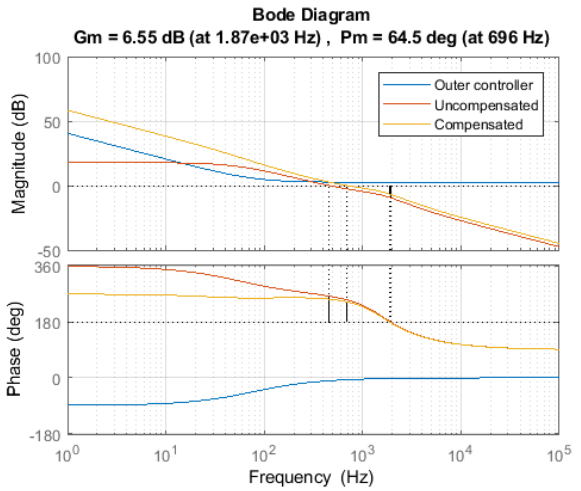

Fig.8. Bode plot of the outer current control loop.

$$G_{pi_1}(z) = \frac{0.28z - 0.214}{z - 1} \quad (20)$$

$$G_{pi_2}(z) = \frac{1.36z - 1.34}{z - 1} \quad (21)$$

V. Experimental Results

The experimental setup shown in Fig. 9 was used to validate the performance of the proposed grid interface current control strategy.

Fig.10 shows the block diagram of the experimental system setup. A battery pack, which has a voltage of 24 V, is connected to the DC bus using a bi-directional battery converter. The proposed grid interface current control was implemented in a TMS320F28335 microcontroller of the battery converter. A DC power supply at current source mode was used in this experiment to represent a PV generation. A DC electronics load was used to represent the DC load within the DC microgrid. Together with a branch resistor load, a DC power supply which has a voltage of 48 V was utilised to represent the main DC grid. All data in the experiment were recorded using an oscilloscope (Wave Runner 104Xi-A). All specifications of the DC microgrid system are presented in Table II.

To experimentally test the proposed grid interface control strategy performance, two cases are studied.

A. Case1: Step Change in Load Current

The objective of this case study is to assess the effects of load disturbances on the grid interface current control. The reference grid interface current value was set as 1A.

As illustrated in Fig.11, the load current at $t = t_1$ was suddenly raised from 0 A to approximately 0.5 A. Consequently, the I_m (grid interface current) proportionally dropped from 1 A to around 0.5 A. In order to maintain the grid interface current I_m at 1 A, the proposed controller increased the battery discharging current from 1 A to 1.5 A. At $t = t_2$ the load current was returned to its original condition. To maintain the grid interface current at 1 A, the controller reduced the battery discharge current from approximately 1.5 A to 1 A.

Fig.12 shows the zoom in the experimental waveforms that occurred at $t = t_1$. This reveals that the grid interface current

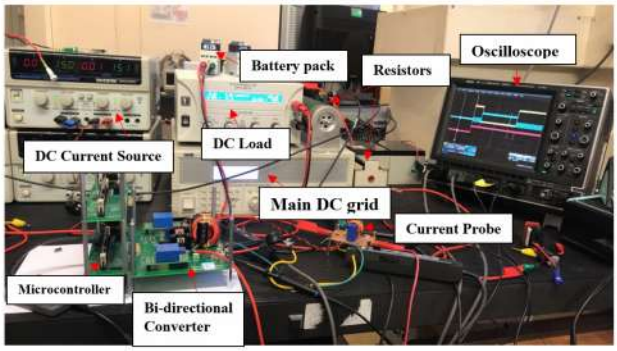

Fig.9. Experimental setup of the DC microgrid system.

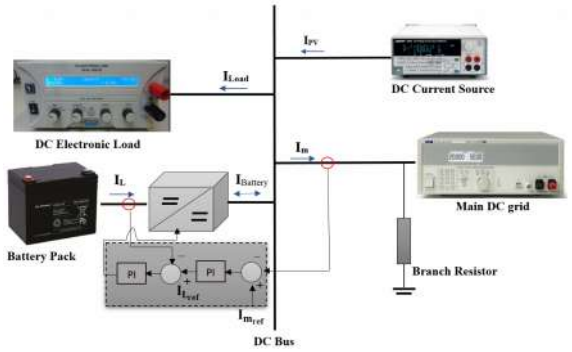

Fig.10.Schematic diagram of the complete DC microgrid system used in the experimental work.

TABLE II
SPECIFICATION OF THE DC MICROGRID SYSTEM

Component	Type	Specification
DC power supply	GW Instek GPS-2303	2 A
Battery pack	YPC33-12×12	24 V
Main DC grid	QPX 1200S 1200-watt DC power supply	48 V
DC electronic load	EA-EL 2400-25	100 Ω
Branch resistors converter	-	10 Ω
Bi-directional converter	-	200W

experienced a step change and then was regulated to 1 A after approximately 75 ms.

The zoom in experimental waveforms at $t = t_2$ is shown in Fig. 13. It shows that the grid interface current has a step change and then was regulated to 1 A after approximately 75 ms.

The performance of the proposed control strategy was compared to that demonstrated in [8] which has an interface converter. It shows that the control in [8] has a different response time vary from 20 ms to 150 ms, which means that the proposed control strategy in this paper has similar performance as [8], and exhibits adequate performance in terms of the rejection of the load current disturbances, while effective regulation of the grid interface current can be achieved without an interface converter.

B. Case2: Step Change in PV Generation

The aim of this case study is to assess the effects of PV disturbances on the grid interface current controller.

In the experiment, a reversed channel scope was used to read the PV current as the assumption was made that the direction of the PV current was opposite to that of the load current. As the PV current injects power to the DC bus, whereas, the load

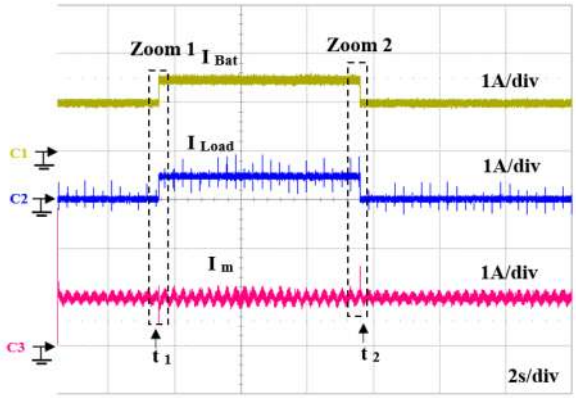

Fig.11.Experimental results for step change in load current.

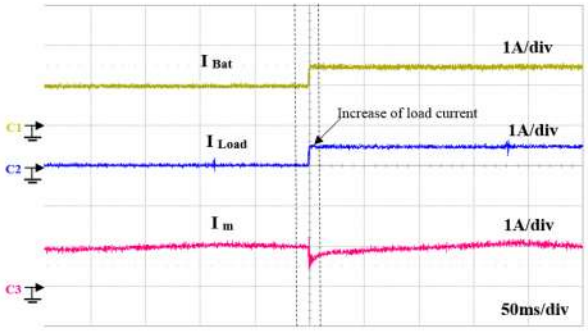

Fig.12. Experimental results for step change in load current under Zoom 1.

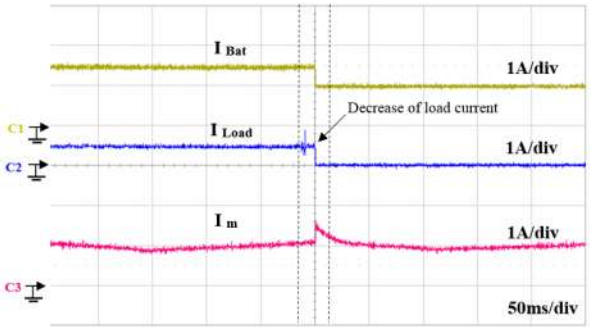

Fig.13. Experimental results for step change in load current under Zoom 2.

current consumes power from the DC bus.

As shown in Fig.14, at the beginning, the PV current was 0 A, and the battery pack was discharged to supply the grid interface current of 1 A. At $t = t_1$, the PV current was raised to 2 A. Consequently, the I_m (grid interface current) is increased from 1 A to approximately 3 A. To maintain the grid interface current I_m at 1 A, the battery was changed to operate in charging mode using a charge current of approximately 1 A for the purpose of absorbing the excess PV supply and regulating the I_m according to its reference value. At $t = t_2$, the PV current was returned to 0 A, and the battery worked as discharging mode with a discharge current of approximately 1 A.

Fig.15 shows the zoom in experimental waveforms at approximately $t = t_1$. It indicates that the grid interface current experiences a step increase change and is then regulated to 1 A after approximately 50 ms.

Fig.16 illustrates the zoom in experimental waveforms at approximately $t = t_2$. It indicates that the grid interface current experiences a step decrease change and is regulated after

approximately 50 ms.

The experimental findings indicate that the grid interface current I_m was maintained at a constant level when variations in the PV current occurred. Hence, the proposed control strategy successfully prevented the PV variations from being transferred to the main DC grid.

C. *Discussion and future work*

From the experimental results, it can be found that battery-based energy storage systems have a relative slow dynamic response to the disturbance from PV generation and the load variation. Also, fast charging/discharging current transition could affect battery lifetime. Therefore, future work will focus on developing a hybrid energy storage solution for this system, which include batteries and supercapacitors.

If the total disturbance current I_R can be measured or estimated, it can be feed-forwarded to the grid interface current controller and improve the dynamic response of the controller. This feed-forward solution will be suitable for a battery current controller with extra current sensors or communication with other power converters.

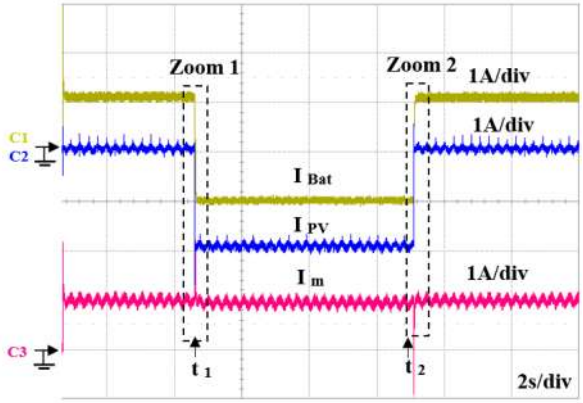

Fig.14.Experimental results for step change in PV generation.

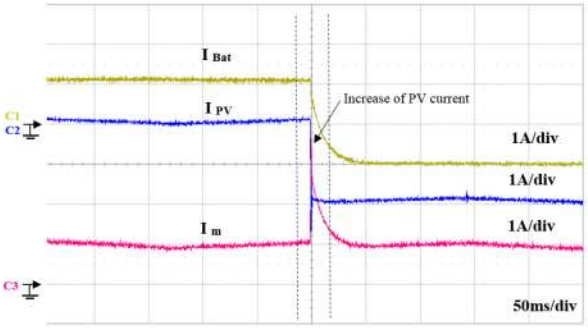

Fig.15. Experimental results for step change in PV generation under Zoom1.

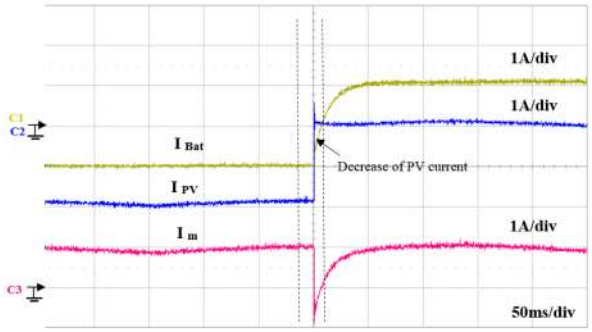

Fig. 16. Experimental results for step change in PV generation under Zoom 2.

VI. CONCLUSIONS

Unpredictable variation of the renewable energy generations and loads could produce negative impact on the main grid. A DC microgrid grid interface current controller has been developed in this research to mitigate the negative effects from the disturbance of PV generation and load demand without a grid interface converter. After an in-depth analysis of the DC-DC converter and interface current control, a double loop grid interface current control is proposed, while both inner and outer current compensators were designed by employing the system transfer functions. The experimental results confirm the effectiveness of the proposed control strategy.

REFERENCES

[1] A. Ipakchi and F. Albuyeh, "Grid of the future," in *IEEE Power and Energy Magazine*, vol. 7, no. 2, pp. 52-62, March-April 2009.

[2] D. Tan, "Structured microgrids: Ultimate assets for utilities," The 11th IET International Conference on Advances in Power System Control, Operation and Management (APSCOM 2018), 2018, pp. 1-7

[3] X. Yu, F. Wang and A. Q. Huang, "Power management strategy for plug and play DC microgrid," 2012 3rd IEEE PES Innovative Smart Grid Technologies Europe (ISGT Europe), Berlin, 2012, pp. 1-7.

[4] J. M. Guerrero, J. C. Vasquez, J. Matas, L. G. de Vicuna and M. Castilla, "Hierarchical Control of Droop-Controlled AC and DC Microgrids—A General Approach Toward Standardization," in IEEE Transactions on Industrial Electronics, vol. 58, no. 1, pp. 158-172, Jan. 2011.

[5] D. Salomonsson, L. Soder and A. Sannino, "Protection of Low-Voltage DC Microgrids," *in IEEE Transactions on Power Delivery*, vol. 24, no. 3, pp. 1045-1053, July 2009.

[6] R. M. Cuzner and G. Venkataramanan, "The Status of DC Micro-Grid Protection," *2008 IEEE Industry Applications Society Annual Meeting*, Edmonton, AB, 2008, pp. 1-8.

[7] Zehir et al., "Impact of Renewable Based Microgrid Supply/Demand Profiles on Low Voltage Distribution Networks", Energy Procedia, vol. 103, pp. 231-236, 2016.

[8] Tricarico, T.; Gontijo, G.; Neves, M.; Soares, M.; Aredes, M.; Guerrero, J.M. Control Design, Stability Analysis and Experimental Validation of New Application of an Interleaved Converter Operating as a Power Interface in Hybrid Microgrids. Energies 2019, 12, 437.

[9] M. Mobarrez, S. Bhattacharya and D. Fregosi, "Implementation of distributed power balancing strategy with a layer of supervision in a low-voltage DC microgrid," *2017 IEEE Applied Power Electronics Conference and Exposition (APEC)*, Tampa, FL, 2017, pp. 1248-1254.

[10] H. Kim and M. Thottan, "A two-stage market model for microgrid power transactions via aggregators", Bell Labs Technical Journal, vol. 16, no. 3, pp. 101-107, 2011.

[11] S. K. Kollimalla, M. K. Mishra and N. L. Narasamma, "Design and Analysis of Novel Control Strategy for Battery and Supercapacitor Storage System," in *IEEE Transactions on Sustainable Energy*, vol. 5, no. 4, pp. 1137-1144, Oct. 2014.

Muhannad Alshareef received the B.Sc. degree in Electrical engineering from Umm-Al-Qura University, Saudi Arabia, in 2011, and the M.Sc. degree in electronics and electrical engineering from Coventry University, UK in 2016. He received the Ph.D degree in electronic engineering from Aston University, UK in 2019. Since 2020, he has been an Assistant Professor with the College of Communication and Electronics Engineering, Umm-Al-Qura

University. His research interests include photovoltaic modeling and control, intelligent control, nonlinear systems control, and optimization techniques such as genetic algorithm, particle swarm optimization, and control and protection of DC microgrid.

Zhengyu Lin (S'03-M'05-SM'10) received the B.Sc. and M.Sc. degrees from the College of Electrical Engineering, Zhejiang University, Hangzhou, China, in 1998 and 2001, respectively, and the Ph.D. degree from Herio-Watt University, Edinburgh, U.K., in 2005. He is currently a Reader in the School of Mechanical, Electrical and Manufacturing Engineering, Loughborough University, Loughborough, UK.

His research interests include power electronics and its applications in renewable energy, energy storage, motor drives, microgrids, and multi-energy systems. He is currently holding an EPSRC UKRI Innovation Fellowship on DC microgrids.

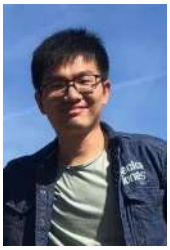

Fulong Li (S'16-M'20) received the B.S. degree in electrical engineering from Yangzhou University, Yangzhou, China, in 2015, and Ph.D. from Aston University, Birmingham, UK, in 2019. He is currently a Research Associate in Loughborough University, U.K.

His current research interests include control and stability analysis of power electronics converters applied in DC microgrids and distributed power systems, and energy management system design of microgrids.

Fei Wang (S'07-M'11-SM'16) received the B.Sc. degree in electrical engineering and the M.Sc. degree in power electronics from Zhejiang University, Hangzhou, China, in 2002 and 2005, respectively, and the Ph.D. degree in power electronics from the Eindhoven University of Technology, Eindhoven, The Netherlands, in 2010. He was with the Philips Lighting Electronics Global Development Center, Shanghai, China, from 2005 to 2006.

He has been a Faculty Member with the School of Mechatronic Engineering and Automation, Shanghai University, Shanghai, since 2010, and became a Professor in March, 2018. He has authored/co-authored more than 100 technical papers, one academic book, and also 13 authorized invention patents. His current research interests include distributed generation, electrical drives, power quality, LED drivers, and smart grid.